Published in final edited form as:

J Neuroendocrinol. 2015 April ; 27(4): 253–263. doi:10.1111/jne.12263.

Chronic oestradiol reduces the dendritic spine density of KNDy (kisspeptin/neurokinin B/dynorphin) neurones in the arcuate nucleus of ovariectomised *Tac2*-enhanced green fluorescent protein transgenic mice

Marina Cholanian[1], **Sally J. Krajewski-Hall**[1], **Nathaniel T. McMullen**[2], and **Naomi E. Rance**[3,*]

[1]Department of Pathology, University of Arizona College of Medicine, Tucson, Arizona, USA

[2]Department of Cellular and Molecular Medicine, University of Arizona College of Medicine, Tucson, Arizona, USA

[3]Department of Pathology, Neurology and the Evelyn F. McKnight Brain Institute University of Arizona College of Medicine, Tucson, AZ, USA

Abstract

Neurones in the arcuate nucleus that express neurokinin B (NKB), kisspeptin and dynorphin (KNDy) play an important role in the reproductive axis. Oestradiol modulates the gene expression and somatic size of these neurones but there is limited information whether their dendritic structure, a correlate of cellular plasticity, is altered by oestrogens. Here we study the morphology of KNDy neurones by filling fluorescent neurones in the arcuate nucleus of *Tac2*-EGFP transgenic mice with biocytin. Filled neurones from ovariectomized (OVX) or OVX plus 17β-oestradiol (E_2)-treated mice were visualized with anti-biotin immunohistochemistry and reconstructed in three dimensions with computer-assisted microscopy. KNDy neurones exhibited two primary dendrites, each with a few branches confined to the arcuate nucleus. Quantitative analysis revealed that E_2 treatment of OVX mice decreased the cell size and dendritic spine density of KNDy neurones. The axons of KNDy neurones originated from the cell body or proximal dendrite and gave rise to local branches that appeared to terminate within the arcuate nucleus. Numerous terminal boutons were also visualized within the ependymal layer of the third ventricle adjacent to the arcuate nucleus. Axonal branches also projected to the adjacent median eminence and exited the arcuate nucleus. Confocal microscopy revealed close apposition of EGFP and GnRH-immunoreactive fibers within the median eminence and confirmed the presence of KNDy axon terminals in the ependymal layer of the third ventricle. The axonal branching pattern of KNDy neurones suggests that a single KNDy neurone could influence multiple arcuate neurones, tanycytes in the wall of the third ventricle, axon terminals in the median eminence and numerous areas outside of the arcuate nucleus. In parallel with its inhibitory effects on electrical excitability, E_2 treatment of OVX *Tac2*-EGFP mice induces structural changes in the somata and dendrites of KNDy neurones.

[*]**CORRESPONDENCE TO:** Naomi E. Rance, MD, PhD, Department of Pathology, University of Arizona College of Medicine, 1501 N. Campbell Ave, Tucson, AZ 85724, USA, nrance@email.arizona.edu, phone: (520) 626-6099.

DISCLOSURE STATEMENT: The authors have nothing to disclose

Keywords

arcuate nucleus; oestrogens; kisspeptin; neurokinins; GnRH; tanycytes

Introduction

In the hypothalamic arcuate (infundibular) nucleus, there is a subpopulation of cells that coexpress oestrogen receptor α and neurokinin B (NKB). These cells are termed KNDy neurones based on the coexpression of kisspeptin, NKB and dynorphin (1). KNDy neurones are modulated by oestrogens in the human (2, 3), monkey (3–5), sheep (6), goat (7), rat (8) and mouse (9, 10). Because both kisspeptin and NKB are essential for pubertal development, gonadotropin secretion and fertility in humans (11, 12), there is intense interest in determining the precise function of KNDy neurones in the reproductive axis. Based on a variety of studies, it has been proposed that KNDy neurones relay the negative feedback effects of oestrogen on gonadotropin secretion (13, 14) and modulate pulses of GnRH secretion from the hypothalamus (7, 15, 16). In addition, KNDy neurones may integrate the reproductive axis with other physiologic systems, such as those regulating body weight (14) and body temperature (17, 18).

In postmenopausal women and ovariectomized monkeys, KNDy neurones undergo cellular hypertrophy accompanied by increased kisspeptin and NKB gene expression (2, 3, 19). Conversely, oestrogen has been shown to decrease the cell body size of kisspeptin neurones in the arcuate nucleus of Kiss1-Cre/GFP mice (10). Although the changes in KNDy neurone size have been well-described, it is not known if this phenomenon is accompanied by structural changes in the dendritic tree. This question is important because changes in the dendritic spine density accompany steroid hormone effects on neurones in many regions of the central nervous system (20–23). In addition, there is virtually no information about the dendritic and axonal architecture of single KNDy neurones. Detailed morphological studies of the arcuate nucleus have been conducted using Golgi impregnation (24), but considering the numerous cell types in the nucleus, these data offer little information on the select population of KNDy neurones. Golgi-like labeling can be obtained in a specific cell type by filling fluorescently-labeled neurones in a tissue slice with biocytin with subsequent immunohistochemical visualization. This single cell approach has been used to study steroid effects on the structure of arcuate neuroendocrine neurones in the rat (25) and GnRH neurones in GnRH-GFP mice (23, 26). Applying this method to the study of KNDy neurones has awaited the development of transgenic mice with reporter genes linked to kisspeptin or NKB promoters.

In the present study, we used tissue slices from *Tac2*-EGFP transgenic mice to study the dendritic and axonal architecture of KNDy neurones. The *Tac2*-EGFP mouse contains a bacterial artificial chromosome in which EGFP is under the transcriptional control of the *Tac2* promoter for NKB (27, 28). In a previous study, 100% of fluorescent neurones in the arcuate nucleus of orchidectomized *Tac2*-EGFP mice expressed *Tac2* and *kiss1* gene transcripts, indicative of the KNDy neurone phenotype (29). Moreover, the onset of puberty, oestrous cycles and oestrogen negative feedback was not altered by the expression of EGFP

in KNDy neurones (30). Finally, E_2 treatment reduced the EGFP signal intensity in the arcuate nucleus of ovariectomized *Tac2*-EGFP mice, similar to the well-described E_2 inhibition of *Tac2* and kisspeptin gene expression in KNDy neurones (8, 31). These data validate the utility of the *Tac2*-EGFP mouse for electrophysiological and morphological studies of KNDy neurones.

To visualize the morphology of KNDy neurones, fluorescent cells in the arcuate nucleus of the *Tac2*-EGFP mouse were filled with biocytin and processed with 3′3′-diaminobenzidine (DAB) immunohistochemistry to produce Golgi-like labeling. *Tac2*-EGFP neurones were then reconstructed in three-dimensions with a Neurolucida computer microscope system and select neurones were drawn with a camera lucida device. We studied chronic estradiol replacement in ovariectomized mice based on our longstanding interest in the effects of estrogen replacement on the morphology of KNDy neurons in postmenopausal women (3, 4, 13). Because chronic E_2 reduces the somatic size, NKB and kisspeptin gene expression and cellular excitability of KNDy neurones in ovariectomized animals (3, 8, 30) we hypothesized that E_2 treatment would also alter the dendritic architecture of KNDy neurones.

Materials and Methods

The *Tac2*-EGFP mouse line was developed by the Gene Expression Nervous System Atlas Project at the Rockefeller University (27, 28). Cryopreserved embryos of *Tac2*-EGFP mice were purchased from the Mutant Mouse Regional Resource Center (015495-UCD; STOCK Tg (*Tac2*-EGFP) 381Gsat/Mmcd, University of California, Davis, CA) and implanted in pseudopregnant females. The experimental animals were generated by breeding heterozygous *Tac2*-EGFP males to wildtype Swiss-Webster females. Litters were genotyped by PCR of tail DNA.

Mice were housed in the Animal Care Facility at the University of Arizona on a 12-h light, 12-h dark cycle (lights on at 0700 h) with water and food available *ad libitum*. Mice were fed a low phytoestrogen-diet (Teklad 2019 Global 19% Protein Extruded Rodent Diet, Harlan Laboratories, Houston, TX). At two months of age, the mice were ovariectomized (OVX) and immediately implanted with SILASTIC capsules (sc, 20-mm effective length, 1.57 mm inner diameter, 3.18 mm outer diameter; Dow Corning, Midland, MI) containing either 180 μg/mL 17β-oestradiol (E_2) dissolved in sesame oil (OVX + E_2) or vehicle (OVX). Capsules were replaced two weeks later. This E_2 replacement regimen has been documented to produce diestrous levels of serum oestradiol (30). The mice were studied at 3 months of age. All protocols were approved by the University of Arizona Institutional Animal Care and Use Committee and conformed to National Institutes of Health guidelines.

Effects of chronic E_2 treatment on the morphology of KNDy neurones in OVX *Tac2*-EGFP mice

Heterozygous *Tac2*-EGFP mice (17 OVX and 20 OVX + E_2) were decapitated under isoflurane anesthesia. The brains were quickly extracted and coronal brain slices (250 μm) were vibratome-sectioned (VT1000P; Leica, Quebec, Canada) in cold (1–2°C), oxygenated artificial cerebrospinal fluid (aCSF, 125 mM NaCl, 24 mM $NaHCO_3$, 1 mM $MgCl_2$, 2.5 mM

KCl, 1 mM $CaCl_2$ and 10 mM D-Glucose, pH 7.3–7.4). Slices were incubated for approximately 2 hours (32°C) in oxygenated aCSF in a slice chamber (Scientific Systems Design Inc., Ontario, Canada). Borosilicate glass pipettes (3–6 MΩ) were pulled (OD: 1.5 mm; ID: 0.75 mm; Sutter Instrument, Novato, CA) and filled with intracellular solution (10 mM HEPES, 0.2 mM EGTA, 6 mM NaCl, 2 mM $MgCl_2$, 130 mM K-gluconate, 4 mM NaATP, 0.4 mM NaGTP, 5 mM glutathione, 0.05 mM spermine, and 1% biocytin, 270–280 mOsm). Tissue slices were transferred to a recording chamber mounted on an Olympus BX-50WI fixed-stage microscope equipped with a 40× water-immersion objective (NA = 0.75). The slices were continuously perfused with oxygenated aCSF at a rate of 1.5 mL/min at ~31.5°C. Fluorescent neurones in the arcuate nucleus were identified by brief fluorescent illumination and then approached with the pipette with the aid of differential interference contrast optics. After obtaining a tight seal (> 1 gigaohm), the membrane was ruptured by quick and gentle suction and whole-cell mode was achieved. The cell was held in voltage-clamp mode for at least 15 minutes (Vhold = −70 mV) to allow biocytin to diffuse from the pipette into the cell. A small number of cells was subjected to additional recording procedures (30) but the majority of cells in the present study were not electrophysiologically characterized. The patch pipette was then detached by gentle withdrawal of negative pressure and the slice was post-fixed overnight in 4% paraformaldehyde (pH 7.4) at 4°C. The slice was rinsed (6 × 10 min) in 0.1 M phosphate-buffered saline (PBS, pH 7.4) and stored in cryoprotectant solution (32) at −20°C until immunocytochemistry.

Immunohistochemistry to visualize biocytin-filled cells—A polyclonal goat anti-biotin antibody (SP 3000, lot number P0710, Vector Laboratories, Burlingame, CA) was used to visualize biocytin-filled cells. Slices were delipidized with descending ethanol solutions (95%, 70%, 50%) followed by rinses in PBS (6 × 10 min). Endogenous peroxidase activity was blocked by 1% H_2O_2 in PBS (30 min), followed by rinses in PBS (2 × 10 min) and PBS with 0.4% Triton X-100 (PBS-TX, 2 × 10 min). Slices were blocked in 5% normal rabbit serum in PBS-TX (60 min), rinsed in PBS-TX (6 × 10 min) and incubated overnight at 4°C with goat anti-biotin (1:10,000) diluted in 5% normal rabbit serum in PBS-TX. The slices were rinsed in PBS-TX (6 × 10 min) and incubated with biotinylated rabbit anti-goat IgG (1:250, Vector Laboratories) diluted in 5% normal rabbit serum in PBS-TX for 2 hours. The slices were then rinsed in PBS-TX (6 × 10 min) and reacted with avidin-biotin complex (1:100 in Vectastain Elite ABC kit, Vector Laboratories) in PBX-TX for 90 min, followed by PBS rinses (6 × 10 min). The slices were preincubated in heavy metal enhanced 3′3′-diaminobenzidine (DAB) (0.05 % DAB, 1% $CoCl_2$, 1% Ni Ammonium sulfate) in PBS for 20 min. The DAB reaction was carried out for 7 min (0.05% DAB, 1% $CoCl_2$, 1% Ni Ammonium sulfate, 0.0045 % H_2O_2) followed by PBS rinses. Slices were cleared in dimethyl sulfoxide (DMSO, 2 × 20 min), transferred into glass jars filled with DMSO and stored in the dark at room temperature. Slices were mounted in DMSO between glass coverslips on custom-made brass rings to minimize tissue shrinkage and enable obverse-reverse brightfield microscopy (33). Coverslips were sealed with Weldit silicone-based adhesive (Ace Hardware) and allowed to dry overnight.

Computer reconstruction of biocytin-filled arcuate KNDy neurones

Sections were coded to prevent experimenter bias. To avoid fading, neurones were traced within two weeks of the immunohistochemical visualization. Neurones with only cell body filling were excluded from analysis. Neurones were manually traced in three dimensions using an image-combining computer microscope system (Microbrightfield, Colchester, VT) equipped with a motorized stage, Neurolucida software and a Zeiss X63 oil-immersion objective (N.A. = 1.25). A Lucivid miniature cathode-ray tube facilitated the tracing by projecting the computer display through the microscope oculars. Measurements through the Z-axis were made with the aid of a Heidenhain Focus Measurement Encoder (Traunreut, Germany) attached to the stage. The contours of the slice were outlined and the neurones digitized in the form of short chords. Endings were encoded as true (ending within section) or truncated at the obverse or reverse face of the tissue section. Spines were defined as all protrusions that extended less than 5 μm from the dendritic shaft (34). Processes greater than 5 μm in length were encoded as branches.

Data Analysis—Neurolucida Explorer software was used to calculate soma area, number of primary dendrites and number of dendritic branches, total dendrite length, dendritic surface area, dendritic volume, and spine density. Analysis of dendritic branch number, total dendritic length, dendritic surface area, and dendritic volume were carried out only on non-truncated dendrites. Statistical comparisons were made using two-tailed Student's *t*-tests. Reconstructed neurones were saved as tiff images and imported into Corel Draw X6 (Corel Inc., Mountainview, CA) for illustrations.

Camera lucida drawings of selected neurones were made with the aid of a Zeiss Standard microscope (Thornwood, NY) equipped with a drawing tube and a Zeiss X63 oil-immersion objective (N.A. = 1.25). Neurones and section borders were traced with a pencil onto white paper. The drawings were retraced using Rapidograph Ultradraw Waterproof ink (Koh-i-noor, Bloomsbury, NJ), digitally scanned as tiff files and imported into Corel Draw X6 for the illustrations.

Confocal microscopy of EGFP and GnRH-ir neurones in *Tac2*-EGFP mice

Fluorescent immunohistochemistry to visualize EGFP and GnRH was combined with a 4′, 6-diamidino-2-phenylindole (DAPI) counterstain to identify ependymal cell nuclei. The polyclonal GFP antibody (GFP-1020, lot no. 1229FP08, Aves Labs, Tigard, OR) was raised in chicken eggs against recombinant GFP emulsified in Freund's adjuvant. A single band around 24 kDA was identified on Western blots of whole mouse embryo homogenates (Aves Labs). This GFP antibody did not label neurones in wildtype mouse tissue (30). The GnRH antibody (PA1–121, Lot no. MD150614, Thermo Scientific, Rockford, IL) was raised in rabbit against a synthetic peptide of mouse GnRH. This antibody produced the expected band on Western blots from mouse brain (35). The neuronal labeling was consistent with the expected distribution and appearance of GnRH neurones visualized with other antibodies (36).

Heterozygous OVX and OVX + E_2 *Tac2*-EGFP mice (n = 6/group) were deeply anesthetized with an overdose of sodium pentobarbital and transcardially perfused with PBS

(pH 7.4), containing 1 unit of heparin/mL, followed by 4% paraformaldehyde in phosphate buffer (pH 7.4). Brains were removed and post-fixed in 4% paraformaldehyde for 4 hours at 4°C and cryoprotected in ascending sucrose solutions in PBS (10%, 20%, 30%) over a three-day interval. The brains were blocked with a mouse brain matrix (Braintree Scientific, Inc., Braintree, MA) and frozen-sectioned on a sliding microtome (40 μm, coronal axis). Sections were stored at −20°C in cryoprotectant solution (32). Unless noted, multiple PBS rinses were performed between each step. Sections were incubated in 0.3% H_2O_2 in PBS for 30 min. After incubation in blocking solution (3% normal goat serum and 0.4% Triton-X in PBS, 1 hour), they were directly incubated in a combination of primary antibodies (chicken anti-GFP, 1:100,000, rabbit anti-GnRH, 1:5,000) in blocking solution (1 hour at 22 °C, then 48 hours at 4 °C). Sections were incubated with biotinylated goat anti-chicken (1:5,000, Vector Laboratories) diluted in the blocking solution for 1 hour followed by avidin-biotin complex (11.25 μl/10 ml) Vectastain Elite ABC kit, Vector Laboratories) for 30 min. Sections were incubated in biotinyl tyramide (1:200, Perkin Elmer, Boston, MA) in PBS with 0.005% H_2O_2 for 20 min and incubated with SA Alexa 488 (1:200, Life Technologies, Grand Island, NY) in PBS with 0.4% Triton-X (3 hours at 37 °C). Sections were stored overnight in PBS at 4 °C. Sections were incubated in goat anti-rabbit conjugated to Alexa 568 (1:500, Life Technologies) in blocking solution for 2 hours. Sections were counterstained with DAPI for 15 min (3 μM DAPI in PBS, Life Technologies) mounted, and coverslipped (0.16 – 0.19 mm thickness, Corning Incorporated, Corning, NY) with ProLong antifade medium (Life Technologies).

Confocal Microscopy—High-contrast image stacks through the mid-level arcuate nucleus and adjacent median eminence of OVX and OVX + E_2 mice (2 sections/mouse, n = 6 mice/group) were obtained using confocal scanning microscopy. The stack images were acquired (0.5 μm z-steps, 400 Hz speed, 2700 × 2700 pixels, pinhole size set at 1 Airy unit) in red, green, and blue channels (405 nm, 488 nm, and 543 nm) using a Leica SP5 Confocal Microscope (Leica Microsystems, Wetzlar, Germany) equipped with Zeiss X40 oil-immersion objective (N.A. = 1.25). Image stacks were automatically montaged (scanfield 2 × 2) to capture the entire arcuate nucleus. Single image montages as well as maximum intensity projections of stack montages were saved as tiff files. Stacks were inspected using Leica Application Suite Advanced Fluorescence software (Leica Microsystems, Wetzlar, Germany). For the illustrations, selected montage stacks were generated from the original tiff files (Metamorph software, Molecular Devices, Sunnyvale, CA). Images were adjusted in Adobe Photoshop (Adobe Systems, San Jose, CA) and exported to Corel Draw Software.

Results

Morphological features of *Tac2*-EGFP neurones in the arcuate nucleus of OVX and OVX + E_2 mice

DAB immunohistochemistry resulted in Golgi-like labeling of biocytin-filled *Tac2*-EGFP neurones. A total of 26 and 15 neurones were filled with biocytin from 14 OVX and 13 OVX + E_2 mice, respectively. Cell filling only labeled a single neurone with no evidence of dye-coupling between neurons. The majority of biocytin-filled cells (OVX, 59%; OVX + E_2, 73%) were located at the mid-level of the arcuate nucleus corresponding to plates 45 to

47 of the mouse atlas (37)(Fig. 1A). Dendrites could be clearly distinguished from axons: thick dendrites emerged from the cell bodies with a gradual tapering of diameter and acute angle dendritic branches. In contrast, the axon of each cell was a thin, frequently beaded structure (ca. 1 μm diameter) without tapering that emerged from the cell body or proximal dendrite and was characterized by right angle branching as well as *en passant* and terminal boutons.

Morphological features of *Tac2*-EGFP neurones are illustrated by the camera lucida drawings in Figs. 1, 2, 3 and 4 and computer-assisted reconstructions in Fig. 5. *Tac2*-EGFP neurones had relatively simple dendritic trees with two primary dendrites and a small number of dendritic branches (Table 1). Total dendritic length was relatively short (ca. 200–300 μm, Table 1) and dendritic fields were restricted to the arcuate nucleus. Qualitatively, neurones could be classified as either spiny or sparsely-spined. There were 27.3 ± 4.3 spines/dendrite on the spiny neurones, compared to 1.8 ± 0.5 spines/dendrite on sparsely-spined neurones (mean ± SEM, n = 23 non-truncated dendrites from 15 spiny neurones in 8 mice, n = 6 non-truncated dendrites from 5 sparsely-spined neurones in 5 mice). The spines were simple protrusions without distinctive morphological features such as bulbous spine heads. In general, the spines on the cell bodies were more variable in size and shape than those on dendrites (Fig. 4).

The axons of *Tac2*-EGFP neurones were complex, with a single beaded axon exhibiting multiple local branches. The axons emerged from a proximal dendrite in the majority of cases (60 % and 75% in OVX and OVX+E_2, respectively) or from the cell body. The axons gave rise to a complex arbor characterized by *en passant* swellings and terminal boutons within the arcuate neuropil (Figs. 1–3). In many neurones, one or two branches of this local plexus extended medially toward the 3rd ventricle with terminal boutons identified within the ependymal layer. Other axonal branches could be followed to terminals in the lateral palisade zone or other areas of the median eminence where they were frequently cut at the surface of the section. Additional projections originating from *Tac2*-EGFP neurones were found exiting the nucleus ventrolaterally or dorsally (Fig. 5). Typically, collateral branches were not observed after the axon exited the arcuate nucleus. In one case, an axon leaving the arcuate nucleus dorsally could be followed to a terminal plexus in the dorsomedial nucleus. Because cells in the present study were examined in coronal slices, the full extent of neurone projections, including their rostral or caudal projections, could not be determined (see Figure 10, Krajewski et al., 2010).

Oestradiol treatment of OVX mice reduces the cell area and dendritic spine density of arcuate *Tac2*-EGFP neurones

The dendritic and axonal morphology of OVX and OVX + E_2 neurones was qualitatively similar with the exception that the OVX neurones appeared to have greater density of both dendritic spines and somatic processes. Quantitative analysis of biocytin-filled *Tac2*-EGFP neurones in OVX and OVX + E_2 *Tac2*-EGFP mice is summarized in Table 1 and Figure 6. The mean cross-sectional area of *Tac2*-EGFP cell bodies was significantly larger in OVX mice relative to OVX + E_2 mice, (Student's *t*-test, $p \leq 0.05$, Fig. 6A). In addition, the dendritic spine density was significantly increased in the OVX group (Student's *t*-test, $p \leq$

0.05, Fig. 6B). In the OVX group, 50 % of the neurones were spiny, compared to 29 % of the neurones in the OVX + E_2 group, but this difference was not statistically significant (Fisher Exact test). Dendritic spines were evenly distributed along the length of the dendrites in both groups. In a few instances there were fewer spines in the most distal portions of the dendrite, however, this was not affected by the steroid treatment. The number of primary dendrites was similar and there was no significant difference in the dendritic spine length between groups (Table 1). Although no significant differences were detected in dendritic length, dendritic surface area or dendritic volume, there was a trend for these values to be greater in the OVX group (Table 1). Because these parameters could only be analyzed on the relatively small number of non-truncated dendrites, these negative results should be interpreted cautiously.

Confocal microscopy of EGFP and GnRH-immunofluorescence in the arcuate nucleus, median eminence and ependymal layer of *Tac2*-EGFP mice

A novel finding in the present study was the identification of axonal branches of *Tac2*-EGFP neurones terminating within the ependymal layer of the third ventricle. To study the relationship between EGFP fibers, ependymal cells and GnRH axons, we combined GFP and GnRH-immunofluorescence with a DAPI nuclear counterstain to reveal ependymal cell nuclei (Fig. 7). The GFP antibody distinctly stained cell bodies and fibers in the arcuate nucleus. Extensive numbers of EGFP fibers were identified within the arcuate nucleus and median eminence, including the lateral palisade zone. Numerous EGFP fiber endings were observed between the DAPI counterstained ependymal nuclei lining the 3rd ventricle (Fig. 7). Thin, beaded GnRH fibers were observed within the arcuate nucleus and the median eminence, with dense innervation of the lateral palisade zone. EGFP fibers were extensively intermingled with GnRH fibers in lateral palisade zone and other areas of the median eminence. Although sparse GnRH fibers were identified in the ependymal layer, the vast majority of EGFP fibers were not closely associated with GnRH processes at this site. No qualitative differences were observed between OVX and OVX + E_2 groups.

Discussion

The present study examined the effects of chronic E_2 on the morphology of KNDy neurones in the arcuate nucleus of ovariectomized *Tac2*-EGFP mice. The use of the *Tac2*-EGFP mouse to study KNDy neurones has been validated previously (29, 30). Golgi-like staining was achieved by biocytin-filling of fluorescent neurones in tissue slices of the arcuate nucleus, followed by DAB immunohistochemistry. A typical KNDy neurone exhibited two primary dendrites whose simple dendritic field was confined to the arcuate nucleus. A single beaded axon originated from the cell body or dendrite and branched extensively to form local collaterals within the arcuate nucleus. Axonal branches also projected to the ventricular surface where they terminated between ependymal lining cells. Other axon collaterals were traced to the median eminence or exited the arcuate nucleus. While the overall dendritic morphology and axonal branching pattern was similar between groups, treatment of ovariectomized mice with E_2 significantly reduced the somatic size and dendritic spine density of KNDy neurones.

The decrease in KNDy spine density by E_2 is noteworthy because dendritic spines are sites of excitatory synaptic inputs, which are most commonly glutamatergic (38, 39). KNDy neurones contain glutamine or its transporter in mice, rat and sheep (40–42) and in the ewe, the majority of synaptic terminals to KNDy neurones are glutamatergic (42). Moreover, a decrease in the density of dendritic spines has been correlated with decreased cellular excitability (43). Consistent with these findings, we have previously shown that E_2 treatment of ovariectomized *Tac2*-EGFP mice reduces the excitability of KNDy neurones to pulses of depolarizing current (30). The reduction in dendritic spines may provide insight into the mechanism whereby oestrogen inhibits LH secretion, a process known as oestrogen negative feedback. Multiple lines of evidence suggest that suppression of LH secretion by E_2 is mediated by inhibiting the activity of KNDy neurones (13, 14). Thus, the inhibitory effect of E_2 on KNDy spine density could ultimately play a role in the inhibition of serum LH by reducing excitatory synaptic input.

In parallel to the decrease in dendritic spine density, E_2 treatment decreased the size of KNDy neurones in *Tac2*-EGFP mice. These findings agree with a previous study showing that E_2 decreases the cell area of arcuate kisspeptin neurones in OVX Kiss1-CRe/GFP mice (10). Conversely, KNDy neurones are larger in response to gonadectomy in male mice (44) ovariectomy of monkeys (3, 5, 19) and KNDy neurones are hypertrophied in postmenopausal women (2, 3). Typically, a change in cell size is directly related to changes in membrane capacitance and, inversely, to input resistance (45) and this correlation has been shown in studies of KNDy neurones (10, 44). However, in our recent electrophysiological studies of the *Tac2*-EGFP mouse, we did not observe a change in input resistance in KNDy after E_2 treatment (30). It is possible that the relatively small change in cell body area described here was insufficient to produce a detectable difference in input resistance. Alternatively, changes in the density, types and location of ionic channels can dramatically affect the input resistance of a given neurone. In postmenopausal women, the neuronal hypertrophy is accompanied by increased Nissl substance, larger nuclei and nucleoli and increased NKB and kisspeptin gene expression (2, 3, 46). It is notable that the effects of gonadal steroids on KNDy cell size are conserved in other species.

Previous anatomic studies in the monkey, rat, sheep and goat have suggested that KNDy neurones form an integrated network in the arcuate nucleus that project to GnRH terminals in the median eminence. Evidence of direct intercommunication between KNDy neurones comes from the demonstration of dual-labeled NKB/kisspeptin-immunoreactive (or NKB/dynorphin) terminals that are closely apposed to KNDy cell bodies (47–49). Moreover, KNDy neurones express the neurokinin 3 receptor (NK_3) the primary receptor for NKB (48, 50) and are activated in tissue slices by NK_3 receptor agonists (29). Finally, tract-tracing studies have shown that KNDy neurones project within the arcuate nucleus (bilaterally) and to the median eminence (49, 51, 52) where NKB or kisspeptin-ir fibers are closely apposed to GnRH terminals (36, 53–55). This interconnected network is postulated to provide an anatomic framework for KNDy neurones to synchronize their activity to coordinate pulsatile release of GnRH (7, 15, 16).

In this study, we observed that KNDy neurones have a complex axonal branching pattern with numerous *en passant* swellings and terminal boutons within the arcuate nucleus. These

findings explain the high density of fibers when the arcuate nucleus is visualized using NKB or kisspeptin immunohistochemistry (48, 55). Axons collaterals of a single KNDy neurone also projected to the median eminence, a site where immunohistochemistry and confocal microscopy revealed closely apposed EGFP and GnRH fibers. Finally, branches extended in a dorsolateral or ventromedial direction outside of the arcuate nucleus, or were cut at the surface of the tissue sections. Because these studies were carried out in coronal tissue sections, we were unable to determine the site of these rostral or caudal projections. However, projections of KNDy neurones to multiple hypothalamic regions have been previously shown using tract-tracing (51, 56), fiber loss after Halasz knife cuts (41) or neonatal MSG injections (51), and mapping dual-labeled fibers (48, 55). Combined with previous studies, our data provides evidence that a single KNDy neurone could influence many other cells within the arcuate nucleus, GnRH terminals within the median eminence and hypothalamic regions outside of the arcuate nucleus. Thus, the axonal branching pattern of KNDy neurones provides a mechanism to coordinate their pulsatile activity, to relay sex-steroid signals to influence GnRH secretion and to integrate the reproductive axis with other physiological systems.

A novel finding in the present study was the identification of axon collaterals of KNDy neurones that terminated within the ependymal layer of the third ventricle. Although the presence of KNDy neurone terminals within the ependymal layer was unexpected, axon terminals were described in this location many decades ago using Golgi stains and electron microscopy (57). The function of the KNDy neurone terminals in the wall of the third ventricle is unknown. GnRH processes have been identified within the ependymal layer (58), but our confocal studies failed to reveal convincing interactions between GFP and GnRH-ir at this site.

The ependymal layer in the wall of the third ventricle is highly specialized. It consists of tanycytes, bipolar cells that are thought to derive from radial glial cells, but express distinct morphologic and molecular characteristics (59). Tanycytes have cell bodies lining the ventricle and long processes arching to the median eminence with end feet terminating on the fenestrated capillaries of the pituitary portal circulation (60). Dynamic interactions among GnRH terminals, tanycytic end feet and endothelial cells are associated with oestrogens effects on GnRH release (61–63). Thus, KNDy neurone projections to the wall of the third ventricle may serve to modulate tanycyte activity, influencing GnRH secretion into the portal capillary system. Alternatively, because tanycytes in this region lack occluding junctions (64), KNDy neurone terminals could release neuropeptides directly into the third ventricle and influence brain function at distant sites.

In summary, biocytin-filling of fluorescent neurones in the arcuate nucleus of *Tac2*-EGFP mice allowed detailed studies of the axonal and dendritic architecture of KNDy neurones. We observed a complex axonal arbor, providing morphological evidence that a single KNDy neurone could influence other cells in the arcuate nucleus, GnRH secretion within the median eminence and other hypothalamic functions. Long-term treatment of OVX mice with physiological levels of E_2 reduced KNDy cell body size and decreased the density of dendritic spines. Thus, E_2 treatment modifies the structure of KNDy neurones, in parallel with the inhibitory effects of E_2 on kisspeptin and NKB gene expression and neuronal

excitability. Given the putative role of KNDy neurones in oestrogen negative feedback, the E_2 reduction of KNDy dendritic spine density could indirectly play a role in the inhibition of serum LH by oestrogens.

Acknowledgments

We are grateful to Drs. Jason Q. Pilarski and Richard Levine for expert electrophysiology advice and Dr. Ralph F. Fregosi for the use of his electrophysiology laboratory.

This study was supported by National Institutes of Health, National Institute on Aging, R01 AG-032315 and RO1 AG047887; M.C. was supported by Science Foundation Arizona, Achievement Rewards for College Scientists Foundation, and The Evelyn F. McKnight Brain Institute. The *Tac2*-EGFP mouse was generated as a part of the Gene Expression Nervous System Atlas project, National Institute of Neurological Disorders and Stroke Contracts N01NS02331 & HHSN271200723701C to The Rockefeller University (New York, NY).

References

1. Goodman RL, Lehman MN, Smith JT, Coolen LM, de Oliveira CVR, Jafarzadehshirazi MR, Pereira A, Iqbal J, Caraty A, Ciofi P, Clarke IJ. Kisspeptin neurons in the arcuate nucleus of the ewe express both dynorphin A and neurokinin B. Endocrinology. 2007; 148:5752–5760. [PubMed: 17823266]
2. Rance NE, Young WS III. Hypertrophy and increased gene expression of neurons containing neurokinin-B and substance-P messenger ribonucleic acids in the hypothalami of postmenopausal women. Endocrinology. 1991; 128:2239–2247. [PubMed: 1708331]
3. Rometo AM, Krajewski SJ, Voytko ML, Rance NE. Hypertrophy and increased kisspeptin gene expression in the hypothalamic infundibular nucleus of postmenopausal women and ovariectomized monkeys. J Clin Endocrinol Metab. 2007; 92:2744–2750. [PubMed: 17488799]
4. Abel TW, Voytko ML, Rance NE. The effects of hormone replacement therapy on hypothalamic neuropeptide gene expression in a primate model of menopause. J Clin Endocrinol Metab. 1999; 84:2111–2118. [PubMed: 10372719]
5. Alçin E, Sahu A, Ramaswamy S, Hutz ED, Keen KL, Terasawa E, Bethea CL, Plant TM. Ovarian regulation of kisspeptin neurones in the arcuate nucleus of the rhesus monkey (Macaca mulatta). J Neuroendocrinol. 2013; 25:488–496. [PubMed: 23331967]
6. Pillon D, Caraty A, Fabre-Nys C, Bruneau G. Short-term effect of oestradiol on neurokinin B mRNA expression in the infundibular nucleus of ewes. J Neuroendocrinol. 2003; 15:749–753. [PubMed: 12834435]
7. Wakabayashi Y, Nakada T, Murata K, Ohkura S, Mogi K, Navarro VM, Clifton DK, Mori Y, Tsukamura H, Maeda K-I, Steiner RA, Okamura H. Neurokinin B and dynorphin A in kisspeptin neurons of the arcuate nucleus participate in generation of periodic oscillation of neural activity driving pulsatile gonadotropin-releasing hormone secretion in the goat. J Neurosci. 2010; 30:3124–3132. [PubMed: 20181609]
8. Rance NE, Bruce TR. Neurokinin B gene expression is increased in the arcuate nucleus of ovariectomized rats. Neuroendocrinology. 1994; 60:337–345. [PubMed: 7529897]
9. Navarro VM, Gottsch ML, Chavkin C, Okamura H, Clifton DK, Steiner RA. Regulation of gonadotropin-releasing hormone secretion by kisspeptin/dynorphin/neurokinin B neurons in the arcuate nucleus of the mouse. J Neurosci. 2009; 29:11859–11866. [PubMed: 19776272]
10. Frazão R, Cravo RM, Donato J Jr, Ratra DV, Clegg DJ, Elmquist JK, Zigman JM, Williams KW, Elias CF. Shift in Kiss1 cell activity requires estrogen receptor alpha. J Neurosci. 2013; 33:2807–2820. [PubMed: 23407940]
11. Topaloglu AK, Reimann F, Guclu M, Yalin AS, Kotan LD, Porter KM, Serin A, Mungan NO, Cook JR, Ozbek MN, Imamoglu S, Akalin NS, Yuksel B, O'Rahilly S, Semple RK. *TAC3* and *TACR3* mutations in familial hypogonadotropic hypogonadism reveal a key role for Neurokinin B in the central control of reproduction. Nat Genet. 2009; 41:354–358. [PubMed: 19079066]

12. Topaloglu AK, Tello JA, Kotan LD, Ozbek MN, Yilmaz MB, Erdogan S, Gurbuz F, Temiz F, Millar RP, Yuksel B. Inactivating *KISS1* mutation and hypogonadotropic hypogonadism. N Engl J Med. 2012; 366:629–635. [PubMed: 22335740]
13. Rance NE. Menopause and the human hypothalamus: evidence for the role of kisspeptin/neurokinin B neurons in the regulation of estrogen negative feedback. Peptides. 2009; 30:111–122. [PubMed: 18614256]
14. Mittelman-Smith MA, Williams H, Krajewski-Hall SJ, Lai J, Ciofi P, McMullen NT, Rance NE. Arcuate kisspeptin/neurokinin B/dynorphin (KNDy) neurons mediate the estrogen suppression of gonadotropin secretion and body weight. Endocrinology. 2012; 153:2800–2812. [PubMed: 22508514]
15. Rance NE, Krajewski SJ, Smith MA, Cholanian M, Dacks PA. Neurokinin B and the hypothalamic regulation of reproduction. Brain Res. 2010; 1364:116–128. [PubMed: 20800582]
16. Lehman MN, Coolen LM, Goodman RL. Minireview: kisspeptin/neurokinin B/dynorphin (KNDy) cells of the arucate nucleus: a central node in the control of gonadotropin-releasing hormone secretion. Endocrinology. 2010; 151:3479–3489. [PubMed: 20501670]
17. Mittelman-Smith MA, Williams H, Krajewsk-Hall SJ, McMullen NT, Rance NE. Role for kisspeptin/neurokinin B/dynorphin (KNDy) neurons in cutaneous vasodilatation and the estrogen modulation of body temperature. Proc Natl Acad Sci U S A. 2012; 109:19846–19851. [PubMed: 23150555]
18. Rance NE, Dacks PA, Mittelman-Smith MA, Romanovsky AA, Krajewski-Hall SJ. Modulation of body temperature and LH secretion by hypothalamic KNDy (kisspeptin, neurokinin B and dynorphin) neurons: A novel hypothesis on the mechanism of hot flushes. Front Neuroendocrinol. 2013; 34:211–227. [PubMed: 23872331]
19. Sandoval-Guzmán T, Stalcup ST, Krajewski SJ, Voytko ML, Rance NE. Effects of ovariectomy on the neuroendocrine axes regulating reproduction and energy balance in young cynomolgus macaques. J Neuroendocrinol. 2004; 16:146–153. [PubMed: 14764001]
20. Gould E, Woolley CS, Frankfurt M, McEwen BS. Gonadal steroids regulate dendritic spine density in hippocampal pyramidal cells in adulthood. J Neurosci. 1990; 10:1286–1291. [PubMed: 2329377]
21. Woolley CS, McEwen BS. Roles of estradiol and progesterone in regulation of hippocampal dendritic spine density during the estrous cycle in the rat. J Comp Neurol. 1993; 336:293–306. [PubMed: 8245220]
22. Calizo LH, Flanagan-Cato LM. Estrogen-induced dendritic spine elimination on female rat ventromedial hypothalamic neurons that project to the periaqueductal gray. J Comp Neurol. 2002; 447:234–248. [PubMed: 11984818]
23. Chan H, Prescott M, Ong Z, Herde MK, Herbison AE, Campbell RE. Dendritic spine plasticity in gonadatropin-releasing hormone (GnRH) neurons activated at the time of the preovulatory surge. Endocrinology. 2011; 152:4906–4914. [PubMed: 21933865]
24. Van den Pol AN, Cassidy JR. The hypothalamic arcuate nucleus of rat - a quantitative Golgi analysis. J Comp Neurol. 1982; 204:65–98. [PubMed: 7056889]
25. Danzer SC, McMullen NT, Rance NE. Dendritic growth of arcuate neuroendocrine neurons following orchidectomy in adult rats. J Comp Neurol. 1998; 390:234–246. [PubMed: 9453667]
26. Campbell RE, Han SK, Herbison AE. Biocytin filling of adult GnRH neurons in situ reveals extensive, spiny, dendritic processes. Endocrinology. 2005; 146:1163–1169. [PubMed: 15564319]
27. Gong S, Zheng C, Doughty ML, Losos K, Didkovsky N, Schambra UB, Nowak NJ, Joyner A, Leblanc G, Hatten ME, Heintz N. A gene expression atlas of the central nervous system based on bacterial artificial chromosomes. Nature. 2003; 425:917–925. [PubMed: 14586460]
28. Heintz N. BAC to the future: the use of bac transgenic mice for neuroscience research. Nat Rev Neurosci. 2001; 2:861–870. [PubMed: 11733793]
29. Ruka KA, Burger LL, Moenter SM. Regulation of Arcuate Neurons Coexpressing Kisspeptin, Neurokinin B, and Dynorphin by Modulators of Neurokinin 3 and κ-Opioid Receptors in Adult Male Mice. Endocrinology. 2013; 154:2761–2771. [PubMed: 23744642]

30. Cholanian M, Krajewsk-Hall SJ, Levine RB, McMullen NT, Rance NE. Electrophysiology of Arcuate Neurokinin B Neurons in Female Tac2-EGFP Transgenic Mice. Endocrinology. 2014; 155:2555–2565. [PubMed: 24735328]
31. Smith JT, Dungan HM, Stoll EA, Gottsch ML, Braun RE, Eacker SM, Clifton DK, Steiner RA. Differential regulation of KiSS-1 mRNA expression by sex steroids in the brain of the male mouse. Endocrinology. 2005; 146:2976–2984. [PubMed: 15831567]
32. Watson RE Jr, Wiegand SJ, Clough RW, Hoffman GE. Use of cryoprotectant to maintain long-term peptide immunoreactivity and tissue morphology. Peptides. 1986; 7:155–159. [PubMed: 3520509]
33. Glaser EM, Van der Loos H. Analysis of thick brain sections by obverse-reverse computer microscopy: application of a new, high clarity golgi-nissl stain. J Neurosci Methods. 1981; 4:117–125. [PubMed: 6168870]
34. Peters A, Kaiserman-Abramof IR. The small pyramidal neuron of the rat cerebral cortex. The perikaryon, dendrites and spines. Am J Anat. 1970; 127:321–355. [PubMed: 4985058]
35. Miller AM, Treloar HB, Greer CA. Composition of the migratory mass during development of the olfactory nerve. J Comp Neurol. 2010; 518:4825–4841. [PubMed: 21031554]
36. Krajewski SJ, Anderson MJ, Iles-Shih L, Chen KJ, Urbanski HF, Rance NE. Morphologic evidence that neurokinin B modulates gonadotropin-releasing hormone secretion via neurokinin 3 receptors in the rat median eminence. J Comp Neurol. 2005; 489:372–386. [PubMed: 16025449]
37. Franklin, KBJ.; Paxinos, G. The mouse brain in stereotaxic coordinates. New York: Elsevier; 2007.
38. McKinney RA, Capogna M, Dürr R, Gähwiler BH, Thompson SM. Miniature synaptic events maintain dendritic spines via AMPA receptor activation. Nat Neurosci. 1999; 2:44–49. [PubMed: 10195179]
39. Segal I, Korkotian I, Murphy DD. Dendritic spine formation and pruning: common cellular mechanisms? Trends Neurosci. 2000; 23:53–57. [PubMed: 10652540]
40. Cravo RM, Margatho LO, Osborne-Lawrence S, Donato J Jr, Atkin S, Bookout AL, Rovinsky S, Fräzao R, Lee CE, Gautron L, Zigman JM, Elias CF. Characterization of Kiss1 neurons using transgenic mouse models. Neuroscience. 2011; 173:37–56. [PubMed: 21093546]
41. Ciofi P, Leroy D, Tramu G. Sexual dimorphism in the organization of the rat hypothalamic infundibular area. Neuroscience. 2006; 141:1731–1745. [PubMed: 16809008]
42. Goodman RL, Coolen LM, Lehman MN. A role for neurokinin B in pulsatile GnRH secretion in the ewe. Neuroendocrinology. 2013; 99:1–15.
43. Leuner B, Shors TJ. New spines, new memories. Mol Neurobiol. 2004; 29:117–130. [PubMed: 15126680]
44. Alreja M. Electrophysiology of kisspeptin neurons. Adv Exp Med Biol. 2013; 784:349–362. [PubMed: 23550014]
45. Johnston, D.; Wu, SM-S. Functional diversity of voltage-gated ionic conductances Foundations of Cellular Neurophysiology. Cambridge: The MIT Press; 1995. p. 183-209.
46. Rance NE, McMullen NT, Smialek JE, Price DL, Young WS III. Postmenopausal hypertrophy of neurons expressing the estrogen receptor gene in the human hypothalamus. J Clin Endocrinol Metab. 1990; 71:79–85. [PubMed: 2370302]
47. Foradori CD, Amstalden M, Goodman RL, Lehman MN. Colocalisation of dynorphin A and neurokinin B immunoreactivity in the arcuate nucleus and median eminence of the sheep. J Neuroendocrinol. 2006; 18:534–541. [PubMed: 16774502]
48. Burke MC, Letts PA, Krajewski SJ, Rance NE. Coexpression of dynorphin and neurokinin B immunoreactivity in the rat hypothalamus: morphologic evidence of interrelated function within the arcuate nucleus. J Comp Neurol. 2006; 498:712–726. [PubMed: 16917850]
49. Wakabayashi Y, Yamamura T, Sakamoto K, Mori Y, Okamura H. Electrophysiological and morphological evidence for synchronized GnRH pulse generator activity among Kisspeptin/neurokinin B/dynorphin A (KNDy) neurons in goats. J Reprod Dev. 2013; 59:40–48. [PubMed: 23080371]
50. Amstalden M, Coolen LM, Hemmerle AM, Billings HJ, Connors JM, Goodman RL, Lehman MN. Neurokinin 3 receptor immunoreactivity in the septal region, preoptic area and hypothalamus of the female sheep: colocalisation in neurokinin B cells of the arcuate nucleus but not in

gonadotrophin-releasing hormone neurones. J Neuroendocrinol. 2010; 22:1–12. [PubMed: 19912479]

51. Krajewski SJ, Burke MC, Anderson MJ, McMullen NT, Rance NE. Forebrain projections of arcuate neurokinin B neurons demonstrated by anterograde tract-tracing and monosodium glutamate lesions in the rat. Neuroscience. 2010; 166:680–697. [PubMed: 20038444]
52. Smith JT, Li Q, Yap KS, Shahab M, Roseweir AK, Millar RP, Clarke IJ. Kisspeptin is essential for the full preovulatory LH surge and stimulates GnRH release from the isolated ovine median eminence. Endocrinology. 2011; 152:1001–1012. [PubMed: 21239443]
53. Goubillon M-L, Forsdike RA, Robinson JE, Ciofi P, Caraty A, Herbison AE. Identification of neurokinin B-expressing neurons as an highly estrogen-receptive, sexually dimorphic cell group in the ovine arcuate nucleus. Endocrinology. 2000; 141:4218–4225. [PubMed: 11089556]
54. Ramaswamy S, Guerriero KA, Gibbs RB, Plant TM. Structural interactions between kisspeptin and GnRH neurons in the mediobasal hypothalamus of the male rhesus monkey (*Macaca mulatta*) as revealed by double immunofluorescence and confocal microscopy. Endocrinology. 2008; 149:4387–4395. [PubMed: 18511511]
55. True C, Kirigiti M, Ciofi P, Grove KL, Smith MS. Characterisation of arcuate nucleus kisspeptin/neurokinin B neuronal projections and regulation during lactation in the rat. J Neuroendocrinol. 2011; 23:52–64. [PubMed: 21029216]
56. Yeo S-H, Herbison AE. Projections of arcuate nucleus and rostral periventricular kisspeptin neurons in the adult female mouse brain. Endocrinology. 2011; 152:2387–2399. [PubMed: 21486932]
57. Millhouse OE. Light and electron microscopic studies of the ventricular wall. Z Zellforsch Mikrosk Anat. 1972; 127:149–174. [PubMed: 5017852]
58. Kozlowski GP, Coates PW. Ependymoneuronal specializations between LHRH fibers and cells of the cerebroventricular system. Cell Tissue Res. 1985; 242:301–311. [PubMed: 3902246]
59. Prevot V, Hanchate NK, Bellefontaine N, Sharif A, Parkash J, Estrella C, Allet C, de Seranno S, Campagne C, de Tassigny X, Baroncini M. Function-related structural plasticity of the GnRH system: a role for neuronal-glial-endothelial interactions. Front Neuroendocrinol. 2010; 31:241–258. [PubMed: 20546773]
60. Langlet F, Mullier A, Bouret SG, Prevot V, Dehouck B. Tanycyte-like cells form a blood-cerebrospinal fluid barrier in the circumventricular organs of the mouse brain. J Comp Neurol. 2013; 521:3389–3405. [PubMed: 23649873]
61. King JC, Rubin BS. Dynamic changes in LHRH neurovascular terminals with various endocrine conditions in adults. Horm Behav. 1994; 28:349–356. [PubMed: 7729803]
62. Prevot V, Croix D, Bouret S, Dutoit S, Tramu G, Stefano GB, Beauvillain JC. Definitive evidence for the existence of morphological plasticity in the external zone of the median eminence during the rat estrous cycle: implication of neuro-glio-endothelial interactions in gonadotropin-releasing hormone release. Neuroscience. 1999; 94:809–819. [PubMed: 10579572]
63. Prevot V, Bellefontaine N, Baroncini M, Sharif A, Hanchate NK, Parkash J, Campagne C, de Seranno S. Gonadotrophin-releasing hormone nerve terminals, tanycytes and neurohaemal junction remodelling in the adult median eminence: functional consequences for reproduction and dynamic role of vascular endothelial cells. J Neuroendocrinol. 2010; 22:639–649. [PubMed: 20492366]
64. Mullier A, Bouret SG, Prevot V, Dehouck B. Differential distribution of tight junction proteins suggests a role for tanycytes in blood-hypothalamus barrier regulation in the adult mouse brain. J Comp Neurol. 2010; 518:943–962. [PubMed: 20127760]

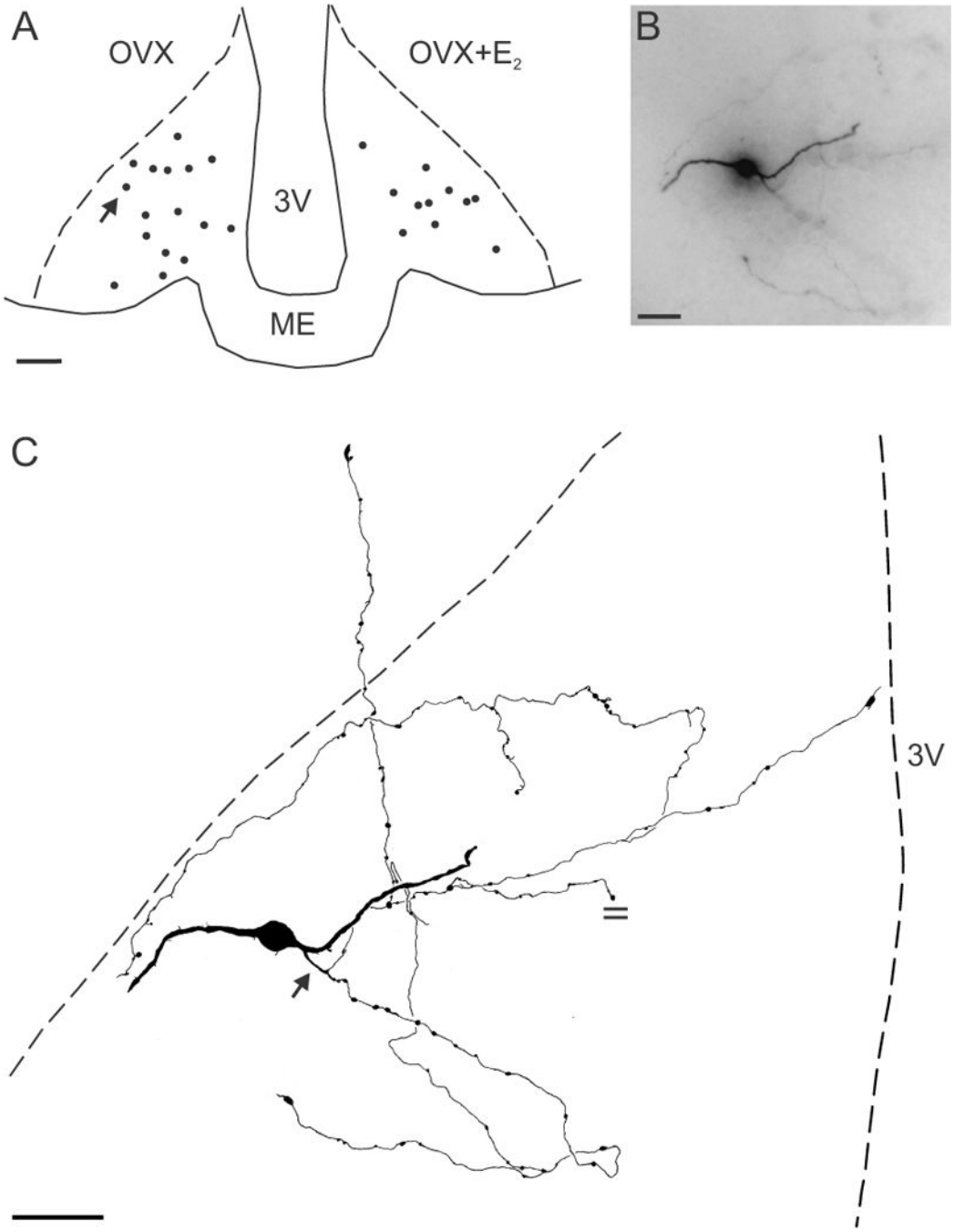

Figure 1.

(A) Computer-assisted map showing the location of biocytin-filled cell bodies at the mid-level of the arcuate nucleus in OVX (left) and OVX+E_2 (right) *Tac2*-EGFP mice. The arrow in A shows the location of the neurone illustrated in B and C. (B) Photomicrograph of a biocytin-filled neurone from an OVX animal reveals a soma (out of focus), two dendrites and an axon arbor out of the focal plane. (C) Camera lucida drawing of the neurone shown in B. This KNDy neurone was spiny with two primary dendrites. The axon (arrow) emerges from a proximal dendrite and gives rise to extensive local collaterals with *en passant* and

terminal boutons within the arcuate nucleus. One axonal branch terminates within the ependymal layer. The parallel lines mark an axon cut at the surface of the section. Scale bar in A = 100 μm, B = 20 μm and C = 50 μm, ME, median eminence, 3V, 3rd ventricle.

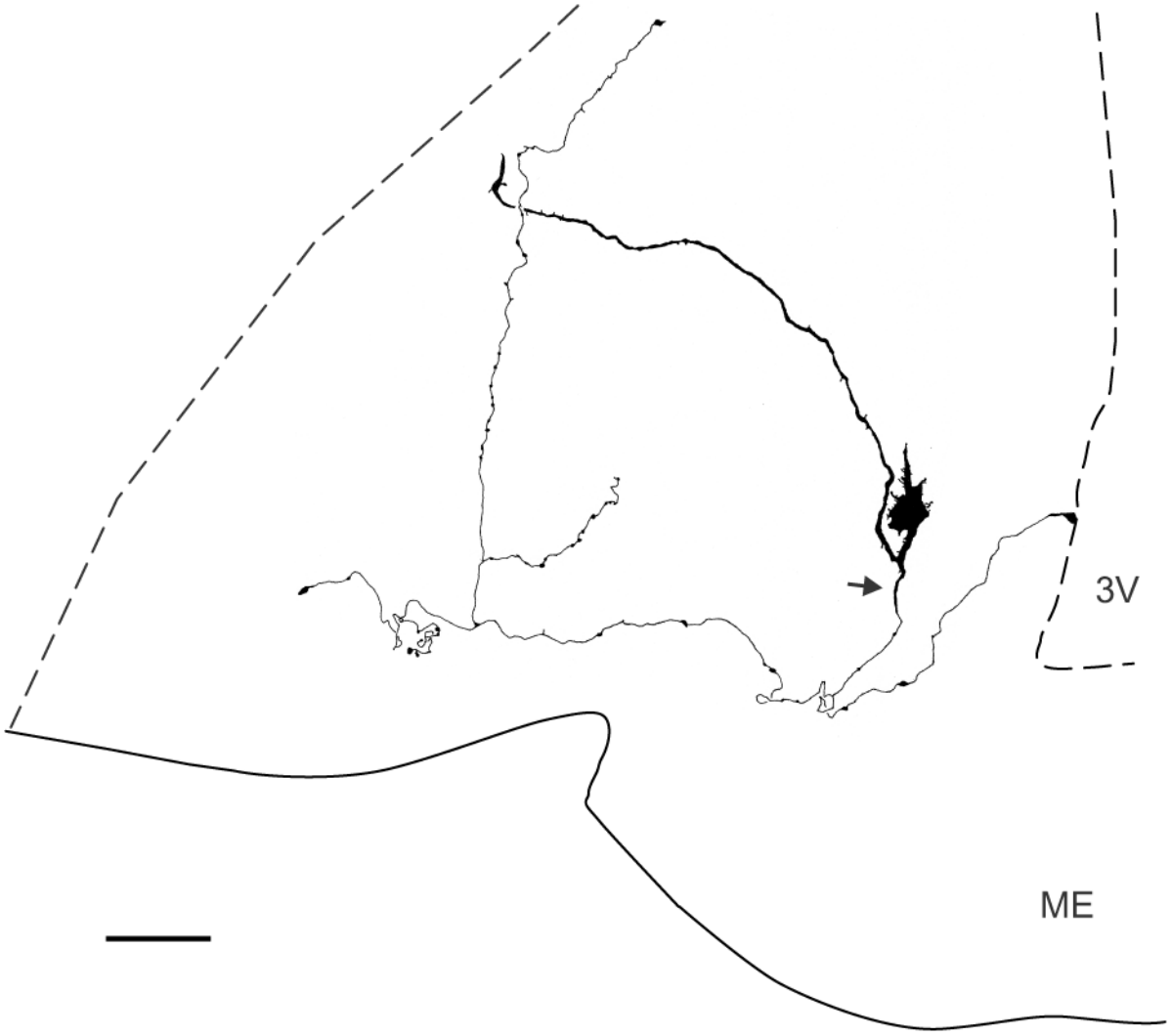

Figure 2.

Camera-lucida drawing of a biocytin-filled KNDy neurone of an OVX *Tac2*-EGFP mouse (mid-level arcuate). This spiny neurone exhibited numerous processes emerging from the soma and a long dendrite that extends nearly to the lateral margin of the nucleus. A beaded axon (arrow) arises from the proximal dendrite and sends local axon collaterals that terminate within the arcuate nucleus and a branch that terminates in the ependymal layer. Scale bar = 50 μm. ME, median eminence, 3V, 3rd ventricle.

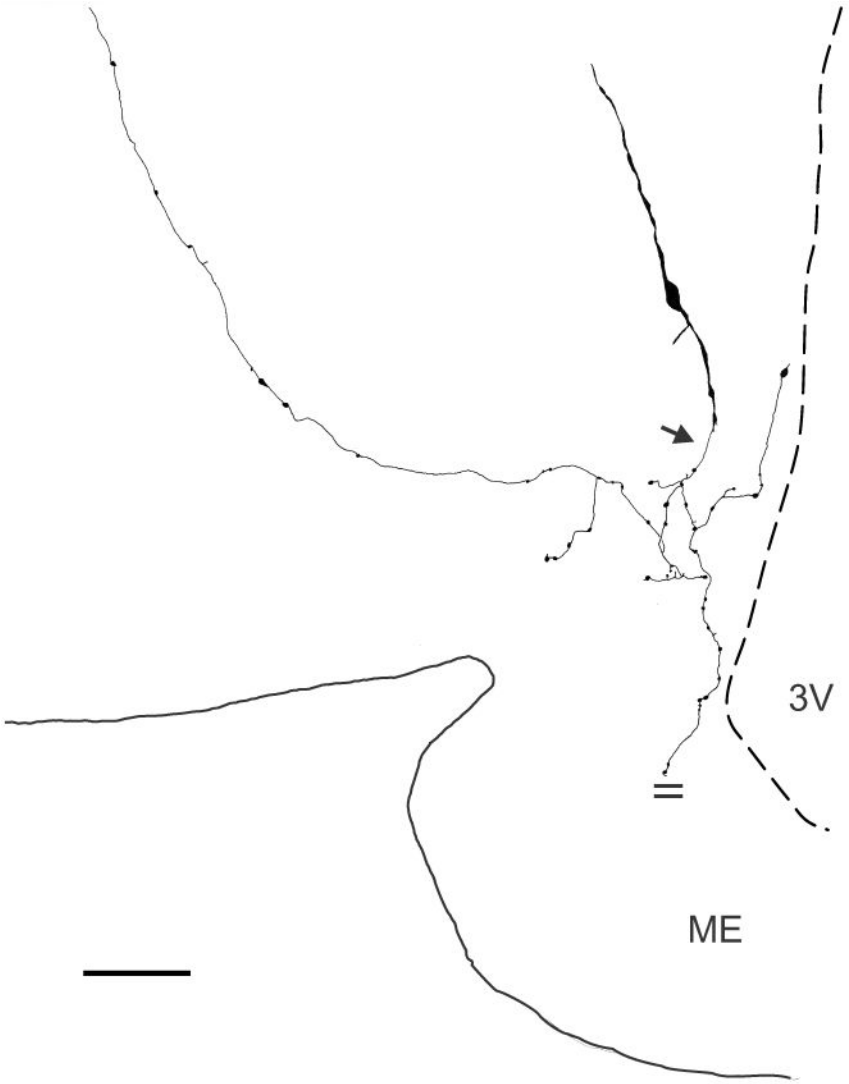

Figure 3.

Camera-lucida drawing of a biocytin-filled KNDy neurone from an OVX + E_2 *Tac2*-EGFP mouse (mid-level arcuate). This neurone is sparsely-spined with two primary dendrites. A beaded axon emerges ventrally (arrow) from a distal dendrite and sends collaterals that terminate within the arcuate nucleus, the ependymal layer of the 3rd ventricle and a dorsolateral branch extending beyond the borders of the arcuate nucleus. An axon collateral extending to the median eminence was cut (parallel lines) at the surface of the tissue slice. Scale bar = 50 μm. ME, median eminence, 3V, 3rd ventricle.

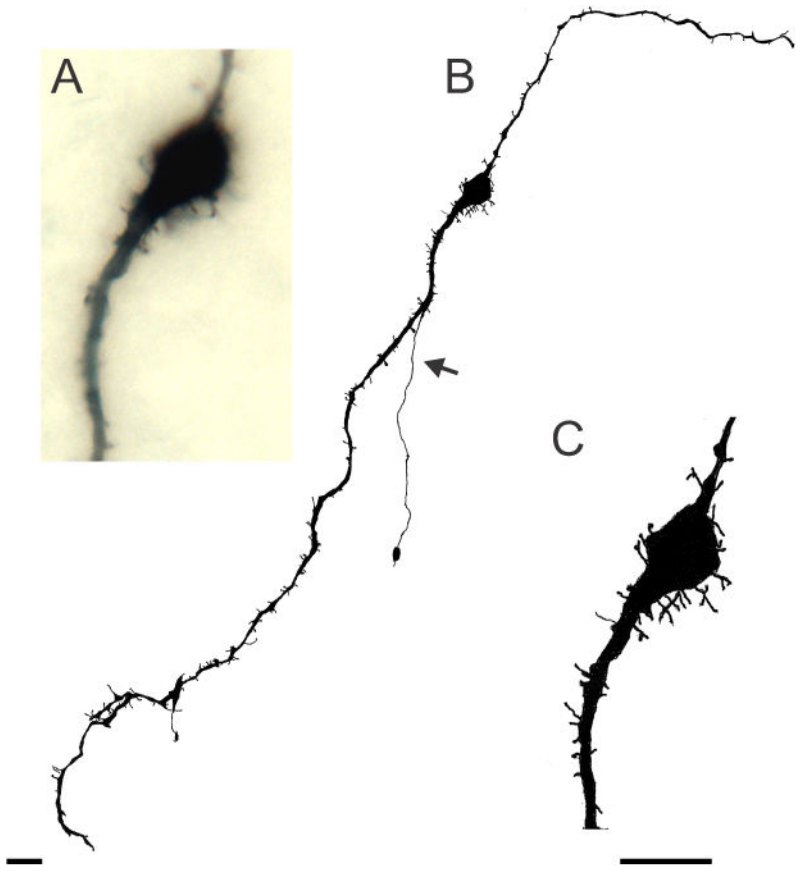

Figure 4.

Spiny KNDy neurone from the anterior arcuate of an OVX *Tac2*-EGFP mouse. (A) Photomicrograph (Zeiss X63 oil-immersion objective, N.A. = 1.25) showing cell body and most of the spines out of the focal plane. (B and C) Camera lucida drawings of the neurone photographed in A. This neurone exhibited numerous somatic and dendritic spines, a few dendritic branches and a simple axon (arrow) originating from a dendrite and terminating within the arcuate nucleus Scale bar in B = 20 μm, Scale bar in C = 20 μm and applies to A and C.

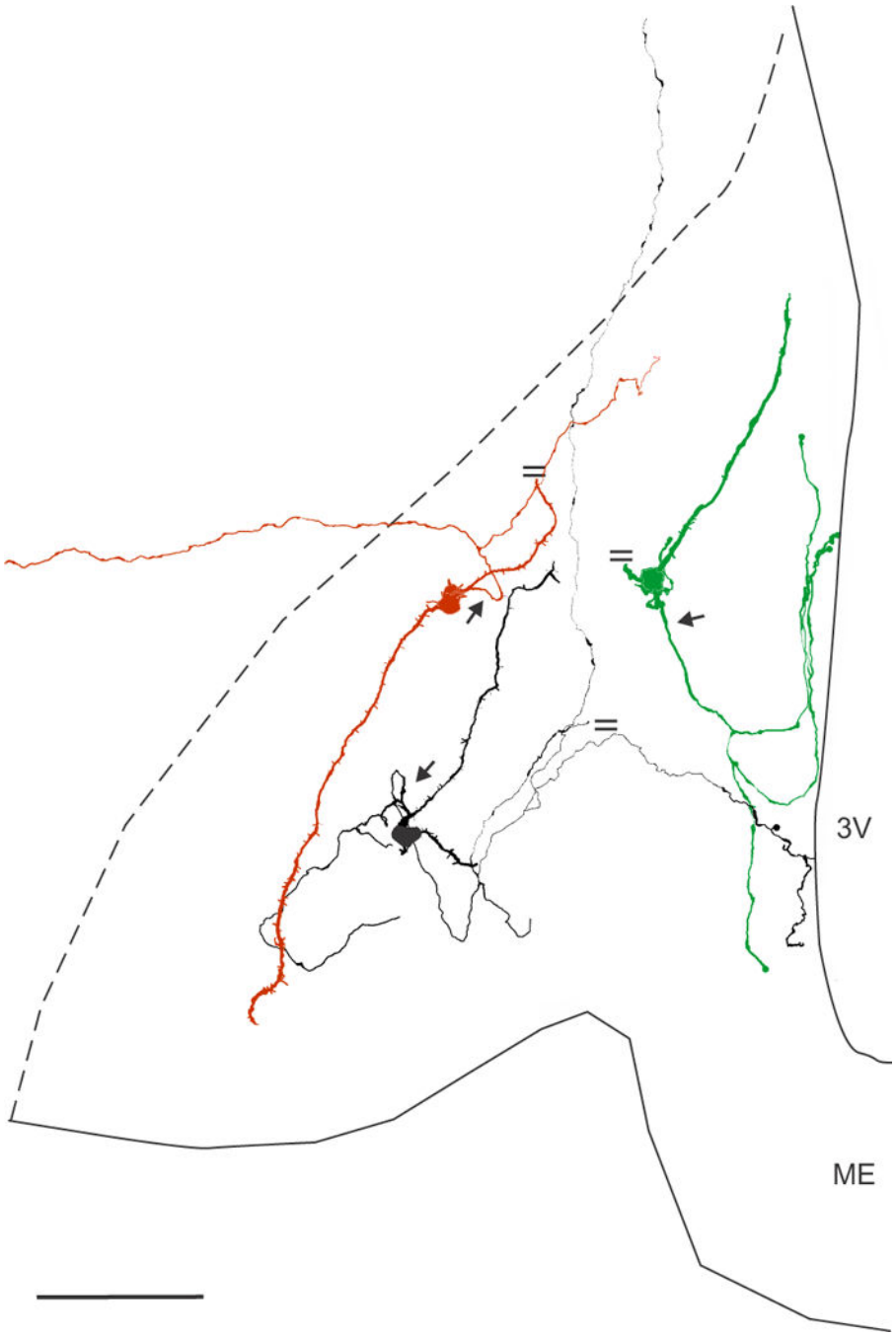

Figure 5.

Neurolucida reconstruction of 3 biocytin-filled KNDy neurones in the arcuate nucleus of OVX *Tac2*-EGFP mice. These neurones digitized from three separate mice, had simple dendritic fields that were restricted to the arcuate nucleus, but different axonal trajectories. The parallel lines indicate cut processes. The axon (arrow) of the red neurone emerged from a proximal dendrite, bifurcated and sent one branch laterally outside of the arcuate nucleus. One of the dendrites was cut at the surface of the section. The axon of the black neurone emerged from a proximal dendrite (arrow) and arborized locally within the arcuate nucleus.

One branch extended dorsally to terminate in an axonal arbor within the dorsomedial nucleus (not shown). One axon was cut at the surface of the section and another branch extended to the wall of the third ventricle. The green neurone had a dendrite that was truncated at the surface of the tissue section and an axon (arrow) emerging from the cell body with branches terminating in the arcuate nucleus and projecting to the ependymal lining. Scale bar = 100 μm. 3V, 3rd ventricle, ME, median eminence.

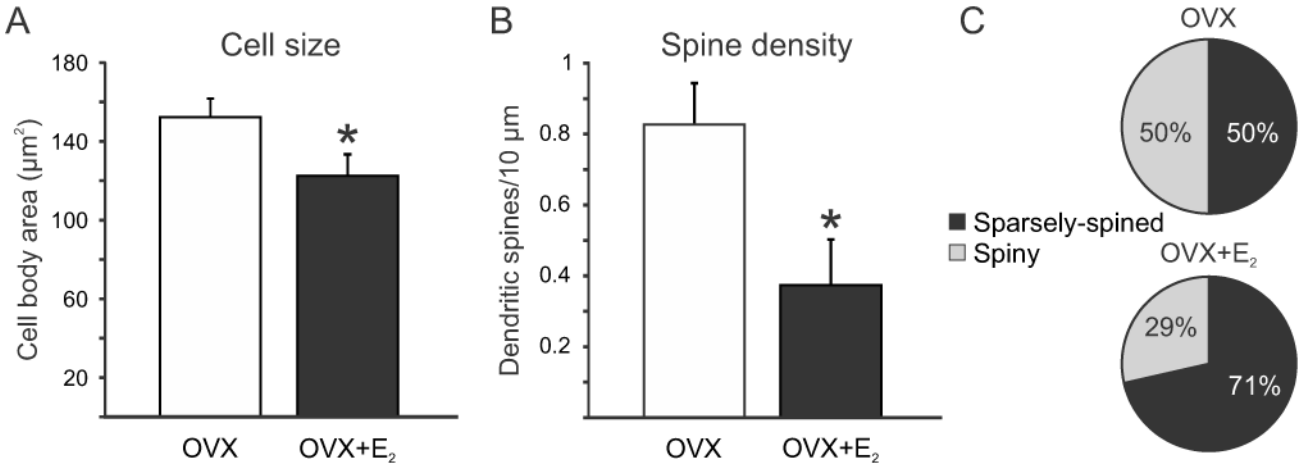

Figure 6.

Effects of chronic oestradiol treatment on the morphology of KNDy neurones in OVX *Tac2*-EGFP mice. (A) Oestradiol treatment significantly reduced the cross-sectional area (A) and dendritic spine density (B) in OVX *Tac2*-EGFP mice. (C) Percentages of sparsely spined and spiny neurones in OVX and OVX + E_2 *Tac2*-EGFP mice. Although more spiny neurones were observed in the OVX mice these values were not significantly different. Values in A and B represent mean ± SEM. For A and C, n = 26 neurones in OVX and 15 neurones in OVX + E_2 mice. For B, n = 39 dendrites in OVX mice and 16 dendrites in OVX + E_2 mice. All data were collected from 14 OVX and 13 OVX + E_2 mice.
*Significantly different, Student's *t*-test, $p \leq 0.05$.

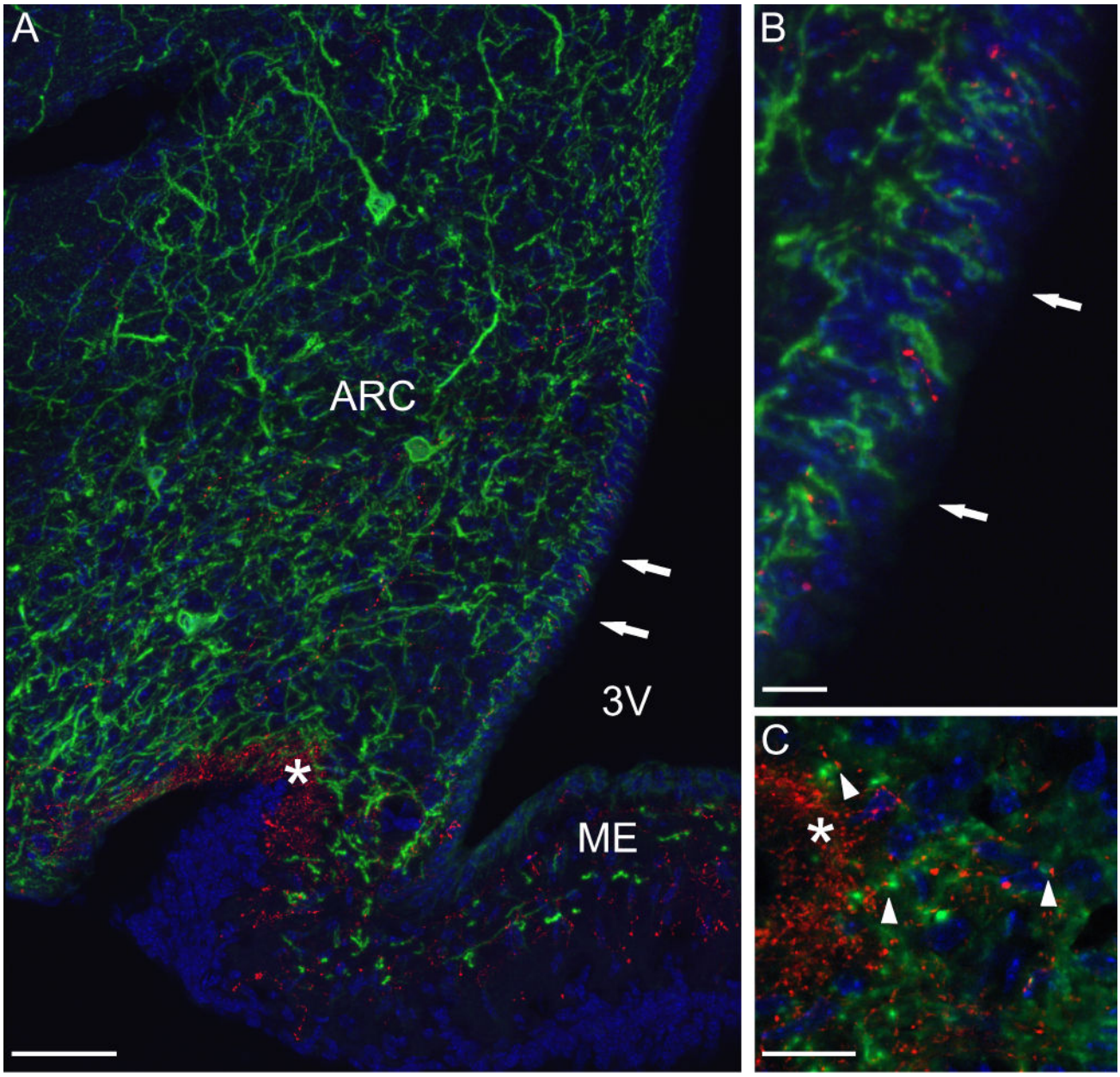

Figure 7.

Confocal microscopy of the arcuate nucleus of *Tac2*-EGFP mice stained with GFP (green) and GnRH (red) antibodies combined with a DAPI-counterstain (blue). (A) Combined projection image of 23 z-steps (z-step 0.5 μm) from an OVX *Tac2*-EGFP mouse. This image shows EGFP cell bodies in the arcuate nucleus with an extensive network of EGFP fibers. EGFP fibers extended to the pial surface at the base of the brain, the ependymal layer of the 3rd ventricle (arrows), the lateral palisade zone (asterisk) and other regions of the median eminence. In the lateral palisade zone, there was extensive intermingling of green EGFP fibers and red GnRH fibers. (B) High magnification confocal image of the ependymal layer marked by arrows in A. Note the finger-like terminations of EGFP fibers within the ependymal lining. (C) Single focal plane (0.5 μm) of the median eminence of an OVX + E_2

mouse showing close apposition (arrowheads) of GFP processes (green) and GnRH axons (red) adjacent to the lateral palisade zone (asterisk). Scale bar on A = 50 μm, on B = 10 μm and on C = 20 μm, ARC, arcuate nucleus, 3V, 3rd ventricle, ME, median eminence.

Table 1

Quantitative analysis of biocytin-filled KNDy neurones in *Tac2*-EGFP mice.

	Primary dendrites	Somatic spines	Dendritic branches	Dendritic length (μm)	Dendritic surface area (μm^2)	Dendritic volume (μm^3)	Spine length (μm)
OVX	2.1 ± 0.1 n = 27 neurones	4.2 ± 0.9 n = 27 neurones	2.1 ± 0.4 n = 21 dendrites	277.4 ± 26.3 n = 21 dendrites	1320.1 ± 146.5 n = 21 dendrites	567.9 ± 74.9 n = 21 dendrites	2.6 ± 0.2 n = 18 neurones
OVX+E_2	2.0 ± 0.2 n = 14 neurones	2.4 ± 1.2 n = 14 neurones	3.5 ± 1.2 n = 8 dendrites	205.6 ± 41.5 n = 8 dendrites	935.3 ± 159.2 n = 8 dendrites	395.0 ± 60.4 n = 8 dendrites	2.4 ± 0.3 n = 8 neurones

Data on primary dendrites and somatic spines are collected from 14 OVX mice and 13 OVX + E_2 mice. Dendritic branches, length, surface area and volume were analyzed only in non-truncated dendrites from 7 OVX and 5 OVX + E_2 mice. Spine length was collected from 9 OVX and 7 OVX + E_2 mice.

Data are presented as mean ± SEM. No significant differences were detected between OVX and OVX + E_2 treated mice (Student's *t*-tests, $\alpha = 0.05$).